1521-009X/12/4005-919–927$25.00
DRUG METABOLISM AND DISPOSITION
Vol. 40, No. 5
43778/3763393

DMD 40:919–927, 2012

Preclinical Disposition of GDC-0973 and Prospective and Retrospective Analysis of Human Dose and Efficacy Predictions

Edna F. Choo, Marcia Belvin, Jason Boggs, Yuzhong Deng, Klaus P. Hoeflich, Justin Ly, Mark Merchant, Christine Orr, Emile Plise, Kirk Robarge, Jean F. Martini,[1] Robert Kassees,[2] Ron G. Aoyama,[3] Atulkumar Ramaiya,[4] and Stuart H. Johnston

Departments of Drug Metabolism and Pharmacokinetics (E.F.C., J.B., Y.D., J.L., E.P.), Cell Signaling Pathways (M.B., K.P.H.), Translational Oncology (M.M., C.O.), and Chemistry (K.R.), Genentech Inc., South San Francisco, California; and Exelixis Inc., South San Francisco, California (J.F.M., R.K., R.G.A., A.R., S.H.J.)

Received November 9, 2011; accepted February 7, 2012

ABSTRACT:

[3,4-Difluoro-2-(2-fluoro-4-iodo-phenylamino)-phenyl]-((*S*)-3-hydroxy-3-piperidin-2-yl-azetidin-1-yl)-methanone (GDC-0973) is a potent and highly selective inhibitor of mitogen-activated protein kinase(MAPK)/extracellular signal-regulated kinase (ERK) 1/2 (MEK1/2), a MAPK kinase that activates ERK1/2. The objectives of these studies were to characterize the disposition of GDC-0973 in preclinical species and to determine the relationship of GDC-0973 plasma concentrations to efficacy in Colo205 mouse xenograft models. The clearance (CL) of GDC-0973 was moderate in mouse (33.5 ml · min^{-1} · kg^{-1}), rat (37.9 ± 7.2 ml · min^{-1} · kg^{-1}), and monkey (29.6 ± 8.5 ml · min^{-1} · kg^{-1}). CL in dog was low (5.5 ± 0.3 ml · min^{-1} · kg^{-1}). The volume of distribution across species was large, 6-fold to 15-fold body water; half-lives ranged from 4 to 13 h. Protein binding in mouse, rat, dog, monkey, and human was high, with percentage unbound, 1 to 6%. GDC-0973-related radioactivity was rapidly and extensively distributed to tissues; however, low concentrations were observed in the brain. In rats and dogs, [^{14}C]GDC-0973 was well absorbed (fraction absorbed, 70–80%). The majority of [^{14}C]GDC-0973-related radioactivity was recovered in the bile of rat (74–81%) and dog (65%). The CL and volume of distribution of GDC-0973 in human, predicted by allometry, was 2.9 ml · min^{-1} · kg^{-1} and 9.9 l/kg, respectively. The predicted half-life was 39 h. To characterize the relationship between plasma concentration of GDC-0973 and tumor growth inhibition, pharmacokinetic-pharmacodynamic modeling was applied using an indirect response model. The KC_{50} value for tumor growth inhibition in Colo205 xenografts was estimated to be 0.389 μM, and the predicted clinical efficacious dose was ~10 mg. Taken together, these data are useful in assessing the disposition of GDC-0973, and where available, comparisons with human data were made.

Introduction

The mitogen-activated protein kinase (MAPK) signaling cascade transduces multiple proliferative and differentiating signals within tumor cells. Four major mammalian MAPK pathway modules have been identified: extracellular signal-regulated kinase 1/2 (ERK1/2), c-Jun NH_2-terminal kinase (JNK), p38 kinase, and ERK5 (Johnson and Lapadat, 2002; Roberts and Der, 2007). Each pathway stimulates different effector pathways. The ERK/MAPK signaling cascade transduces multiple proliferation and differentiation signals within the cell via activation of the RAS GTPase and subsequent sequential activation of RAF, MAPK/ERK kinase (MEK), and ERK kinases. Aberrant regulation of this pathway contributes to many hallmarks of cancer cells, including uncontrolled proliferation, invasion, metastasis, angiogenesis, and evasion of apoptosis (Downward, 2003; Roberts and

[1] Current affiliation: Pfizer Inc., La Jolla, California.
[2] Current affiliation: Genentech Inc., South San Francisco, California.
[3] Current affiliation: Rigel Pharmaceuticals Inc., South San Francisco, California.
[4] Current affiliation: University of Illinois, Chicago, Illinois.

Article, publication date, and citation information can be found at http://dmd.aspetjournals.org.
http://dx.doi.org/10.1124/dmd.111.043778.

ABBREVIATIONS: MAPK, mitogen-activated protein kinase; ERK, extracellular signal-regulated kinase; JNK, c-June NH_2-terminal kinase; MEK, MAPK/ERK kinase; P-gp, P-glycoprotein; GDC-0973, [3,4-difluoro-2-(2-fluoro-4-iodo-phenylamino)-phenyl]-((*S*)-3-hydroxy-3-piperidin-2-yl-azetidin-1-yl)-methanone; GDC-0941, 2-(1*H*-indazol-4-yl)-6-[[4-(methylsulfonyl)-1-piperazinyl]methyl]-4-(4-morpholinyl)-thieno[3,2-d]pyrimidine; GSK1120212, *N*-{3-[3-cyclopropyl-5-(2-fluoro-4-iodophenylamino)-6,8-dimethyl-2,4,7-trioxo-3,4,6,7-tetrahydro-2*H*-pyrido[4,3-d]pyrimidin-1-yl]phenyl}acetamide; PI3K, phosphatidylinositol 3-kinase; AS703026, (*S*)-*N*-(2,3-dihydroxypropyl)-3-((2-fluoro-4-iodophenyl)amino)isonicotinamide; RDEA119, (*R*)-*N*-(3,4-difluoro-2-(2-fluoro-4-iodophenylamino)-6-methoxyphenyl)-1-(2,3-dihydroxypropyl)cyclopropane-1-sulfonamide; TAK-733, 3-[(2*R*)-2,3-dihydroxypropyl]-6-fluoro-5-(2-fluoro-4-iodoanilino)-8-methylpyrido[2,3-*d*]pyrimidine-4,7-dione; MDCK, Madin-Darby canine kidney; A-B, apical-to-basolateral; B-A, basolateral-to-apical; ER, efflux ratio; pERK, phosphorylated extracellular signal-regulated kinase; PK, pharmacokinetics; CL, clearance; LC-MS/MS, liquid chromatography/tandem mass spectrometry; AUC_{inf}, area under the plasma concentration-time curve from time 0 extrapolated to infinity; QWBA, quantitative whole-body autoradiography; BDC, bile duct cannulated; PD, pharmacodynamics; PK, pharmacokinetic; MLP, maximal life-span potential; AUC, area under the curve; TGI, tumor growth inhibition; *F*, bioavailability; AAG, α-1-acid glycoprotein; HSA, human serum albumin; MDR1, multidrug resistance 1; MCT, methylcellulose/0.2% (v/v) Tween 80; RO4987644, 3,4-difluoro-2-((2-fluoro-4-iodophenyl)amino)-*N*-(2-hydroxyethoxy)-5-((3-oxo-1,2-oxazinan-2-yl)methyl)benzamide.

Der, 2007). Inhibition of MEK is a promising strategy in the development of oncology therapeutics to control the growth of tumors that are dependent on aberrant ERK/MAPK pathway signaling (Wellbrock et al., 2004; Solit et al., 2006; Hoeflich et al., 2008).

[3,4-Difluoro-2-(2-fluoro-4-iodo-phenylamino)-phenyl]-((*S*)-3-hydroxy-3-piperidin-2-yl-azetidin-1-yl)-methanone (GDC-0973) (Fig. 1) is an allosteric inhibitor of MEK1/2, with a MEK1 IC_{50} of 4.2 nM. It shows >100× selectivity against >100 kinases (Belvin et al., 2010). In Colo205 cells (BRAF V600E mutant), the IC_{50} values associated with cellular inhibition of ERK1/2 phosphorylation and proliferation were 1.8 and 8 nM, respectively. Cellular inhibition of ERK1/2 was also observed in other tumor cell lines that are dependent on aberrant ERK/MAPK pathway signaling, e.g., harboring the BRAF and KRAS mutation(s). In addition, in vivo efficacy is observed in BRAF and KRAS mutant cell lines both as a single-agent GDC-0973 and in combination with 2-(1*H*-indazol-4-yl)-6-[[4-(methylsulfonyl)-1-piperazinyl]methyl]-4-(4-morpholinyl)-thieno[3,2-d]pyrimidine (GDC-0941) (Hoeflich et al., 2009; Belvin et al., 2010; Rosen et al., 2011). GDC-0973 is currently undergoing oncology clinical trials both as a single agent and in combination with GDC-0941 (phosphatidylinositol 3-kinase [PI3K] inhibitor) and vemurafenib (BRAF inhibitor) (National Institutes of Health, www.clinicaltrials.gov). The effort to modulate MEK is a competitive area of research as evidenced by the multiple MEK inhibitors at various stages of clinical development, e.g., AZD6244, AZD8330, (*S*)-*N*-(2,3-dihydroxypropyl)-3-((2-fluoro-4-iodophenyl)amino)isonicotinamide (AS703026), *N*-{3-[3-cyclopropyl-5-(2-fluoro-4-iodophenylamino)-6,8-dimethyl-2,4,7-trioxo-3,4,6,7-tetrahydro-2*H*-pyrido[4,3-d]pyrimidin-1-yl]phenyl}acetamide (GSK1120212), (*R*)-*N*-(3,4-difluoro-2-(2-fluoro-4-iodophenylamino)-6-methoxyphenyl)-1-(2,3-dihydroxypropyl)cyclopropane-1-sulfonamide (RDEA119), RO4987644, and 3-[(2*R*)-2,3-dihydroxypropyl]-6-fluoro-5-(2-fluoro-4-iodoanilino)-8-methylpyrido[2,3-d]pyrimidine-4,7-dione (TAK-733) (Frémin and Meloche, 2010).

The objective of the studies/data presented here was to characterize the disposition of GDC-0973 in preclinical species and to determine the relationship of GDC-0973 plasma concentrations to efficacy in Colo205 (V600E; colon) mouse xenograft models. Where available, comparisons are made to observed human data.

Materials and Methods

Chemicals and Reagents. GDC-0973 was synthesized by Exelixis Inc. (South San Francisco, CA) and Genentech Inc. (South San Francisco, CA). [^{14}C]GDC-0973 (radiochemical purity >98%) was synthesized at Ricerca (Solon, OH). All other reagents or material used in these studies were purchased from Sigma-Aldrich (St. Louis, MO) unless otherwise stated.

In Vitro Studies. *MDCK cell permeability.* The MDCKI cell line was acquired from American Type Culture Collection (Manassas, VA). GDC-0973 was added to either the apical or the basolateral side of the monolayer at an initial concentration of 10 μM and was incubated at 37°C for 90 min. The apparent permeability (P_{app}), in the apical-to-basolateral (A-B) and basolateral-to-apical (B-A) directions, was calculated as $P_{app} = (dQ/dt) \cdot (1/AC_0)$, where dQ/dt = rate of compound appearance in the receiver compartment; A = surface area of the insert; C_0 = initial substrate concentration at time = 0. The efflux ratio (ER) was calculated as ($P_{app,\ B\text{-}A}/P_{app,\ A\text{-}B}$).

MDR1-MDCK permeability. The assay was conducted by Absorption Systems LP (Exton, PA). In the substrate assay, concentrations of 25 μM GDC-0973 or 10 μM digoxin (positive control) were used. In some studies, the assay buffer also contained 10 μM cyclosporine A or 25 μM GDC-0973 as potential P-glycoprotein (P-gp) inhibitors. After the preincubation period, cell monolayers were dosed on the apical side (A-to-B) or basolateral side (B-to-A) and were incubated at 37°C with 5% CO_2 in a humidified incubator for 2 h. After 2 h of incubation, samples were taken from the donor chambers. All samples were assayed by liquid chromatography/tandem mass spectrometry (LC-MS/MS). The P_{app} values were calculated as follows: $P_{app} = (dC_r/dt) \times V_r/(A \times C_N)$, where dC_r/dt is the slope of the cumulative concentration in the receiver compartment versus time in μM s^{-1}; V_r is the volume of the receiver compartment in cm^3; V_d is the volume of the donor compartment in cm^3; A is the area of the cell monolayer (1.13 cm^2 for 12-well Transwell plates); C_N is the nominal concentration of the dosing solution in μM.

Blood-to-plasma partitioning. The blood-to-plasma partitioning of GDC-0973 was assessed in pooled whole blood from CD-1 mice, Sprague-Dawley rats, beagle dogs, cynomolgus monkeys, and humans (Bioreclamation, Inc., Hicksville, NY). Blood from all species was obtained from at least three individual donors. The blood-to-plasma partitioning of GDC-0973 and [^{14}C]GDC-0973 was determined at whole-blood concentrations of 1, 5, and 10 μM. Blood samples were incubated at 37°C for 30 min in a shaking water bath. The blood-to-plasma ratio was calculated by dividing the measured radioactivity in blood by that measured in plasma. Incubations were performed in quadruplicate. Parameters are presented as mean ± S.D.

Plasma protein binding. The extent of plasma protein binding of GDC-0973 was determined in vitro, in mouse, rat, monkey, dog, and human plasma (Bioreclamation, Inc.), as well as human serum albumin (HSA; 40 mg/ml) and α-1-acid glycoprotein (AAG; 1 mg/ml) by equilibrium dialysis using an HTDialysis 96-well block (HTDialysis LLC, Gales Ferry, CT), as described previously (Choo et al., 2009). GDC-0973 and [^{14}C]GDC-0973 were added to pooled plasma ($n \geq 3$) at total concentrations of 1, 5, and 10 μM. Plasma samples were equilibrated with phosphate-buffered saline (pH 7.4) at 37°C in 90% humidity and 5% CO_2 for 5 h. The percentage GDC-0973 unbound in plasma was determined by dividing the radioactivity measured in the postdialysis buffer by that measured in the post-dialysis plasma and multiplying by 100. Incubations were performed in quadruplicate. Parameters are presented as mean ± S.D. Using a similar method, brain binding of GDC-0973 was determined as described previously (Kalvass et al., 2007).

Metabolic stability study in liver microsomes. The oxidative metabolism of GDC-0973 was evaluated in pooled liver microsomes (Celsis, Chicago, IL) of CD-1 mice, Sprague-Dawley rats, cynomolgus monkeys, beagle dogs, and humans (Invitrogen, Carlsbad, CA) as described previously (Salphati et al., 2011). The Incubation mixture contained 0.5 mg/ml microsomal protein and 1 μM GDC-0973. Reaction was initiated with the addition of NADPH. Samples were incubated at 37°C, aliquots were sampled at 0, 20, 40, and 60 min, and the percentage of GDC-0973 remaining was determined by LC-MS/MS using the $t = 0$ peak area ratio values as 100%. The in vitro intrinsic clearance and scaled hepatic clearance (CL) were determined as described by Obach et al. (1997).

In Vivo Studies. Studies were performed at Genentech Inc. by Exelixis, Covance Laboratories (Madison, WI, Kalamazoo, MI, or Alice, TX), or QPS LLC (Newark, DE). Food and water were available ad libitum except for animals that were administered oral doses in pharmacokinetic (PK) studies, which were fasted overnight before dosing of GDC-0973. In all studies, blood samples were collected in tubes containing K_2EDTA as the anticoagulant. Plasma was isolated and stored at −80°C until analysis. The concentration of GDC-0973 in each plasma and/or tissue sample was determined by LC-MS/MS analysis.

PK study in mouse. Twenty-seven female nu/nu mice (Charles River Laboratories, Inc., Wilmington, MA) were given a 1 mg/kg i.v. dose (4 ml/kg dosing volume) of GDC-0973 hydrochloride (HCl) salt in 60% propyl ethylene glycol 400 (60% v/v) and water (40% v/v). Another group of 27 mice at each dose level received 3, 10, and 30 mg/kg p.o. (4 ml/kg dosing volume) of GDC-0973, formulated in 0.5% (w/v) methylcellulose/0.2% (v/v) Tween-80 (MCT). At the initiation of the study, the mice weighed from 20 to 27 g. One

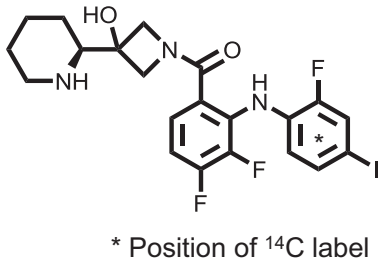

FIG. 1. Chemical structure of GDC-0973.

blood sample of approximately 0.2 ml was collected from each mouse ($n = 3$ mice per time point) by terminal cardiac puncture, under anesthesia with isoflurane. Blood samples were collected at predose and at 0.033, 0.16, 0.5, 1, 3, 6, 9, and 24 h after the intravenous administration, and at predose and at 0.083, 0.25, 0.5, 1, 3, 6, 9, and 24 h after the oral dose.

In additional studies, GDC-0973 was administered at 3 mg/kg p.o. (dosing volume 4 ml/kg) to nu/nu mice. Brain and plasma were collected 2, 6, 10, 24, and 48 h ($n = 3$/time point) after the fifth dose, to take into consideration any possible accumulation and extended half-life in tissue and to ensure that sampling occurred at steady state. In addition to concentrations of GDC-0973 in brain, phosphorylated extracellular signal-regulated kinase (pERK) levels (as a biomarker of target knockdown) in brain tissue were determined. In another separate study, brain, tumor (Colo205), and plasma were collected from mice at 2 h ($n = 3$). All collected blood samples were centrifuged within 1 h of collection, and plasma was collected and stored at −80°C until analysis. Brain and tumor were homogenized in 3 volumes of water.

PK study in rat. Jugular vein-cannulated female CD rats (12 weeks old, ~200 g) were purchased from Taconic Farms (Germantown, NY). Animals were acclimatized for 48 h before study initiation. Four rats were each given a single intravenous or oral dose of 3 mg/kg (10 ml/kg dosing volume) GDC-0973 HCl salt in 0.9% normal saline. Blood samples (approximately 0.2 ml/sample) were drawn from each animal via the jugular vein cannulae at predose and at 0.02, 0.08, 0.25, 0.5, 1, 2, 4, 8, 12, and 24 h postdose. The samples were collected into tubes containing K_2EDTA as an anticoagulant. Plasma was isolated and kept at −80°C until analysis. The concentration of GDC-0973 in plasma was determined by LC-MS/MS.

PK study in cynomolgus monkey. Six male cynomolgus monkeys (3.5–4.7 kg; Covance Laboratories) were administered GDC-0973 HCl. Three animals each were administered an intravenous (3 mg/kg) and oral (3 mg/kg) dose. GDC-0973 dose solutions were prepared in 0.9% normal saline and were administered at a dosing volume of 1 ml/kg. Blood samples (~1 ml/sample) were collected from the femoral vein at predose and at 0.083, 0.25, 0.5, 1, 2, 3, 4, 6, 8, 12, 24, and 48 h after intravenous and oral dose administration.

PK study in beagle dogs. Six male Beagle dogs (Covance Laboratories; 10.0–11.1 kg) were administered GDC-0973 as the HCl salt. Three animals each were administered an intravenous (3 mg/kg) and oral (3 mg/kg) dose. GDC-0973 dose solutions were prepared in 0.9% normal saline and were administered at a dosing volume of 1 ml/kg. Blood samples (~2 ml) were collected from the jugular vein at predose and at 0.083, 0.25, 0.5, 1, 2, 4, 6, 8, 12, 24, and 48 h after intravenous and oral dose administration.

LC-MS/MS Analysis. GDC-0973 concentrations were determined by LC-MS/MS after protein precipitation with acetonitrile and injection of the supernatant onto the column. The column was an Eclipse XBD-C18 (50 × 4.6 mm, 5-μm particle size) (Agilent Technologies, Santa Clara, CA). A CTC HTS PAL autosampler (LEAP Technologies, Carrboro, NC) linked to a Shimadzu LC-10AD pump (Shimadzu, Columbia, MD), coupled with a Sciex API 4000 triple quadrupole mass spectrometer (Applied Biosystems, Foster City, CA), was used for the LC-MS/MS assay. The aqueous mobile phase was water with 0.1% formic acid, and the organic mobile phase was acetonitrile with 0.1% formic acid. The total run time was 3 min, and the ionization was conducted in the positive-ion mode using the transition m/z 530.25 → 126.75. The lower and upper limits of quantitation of the assay were 0.004 and 40 μM, respectively. The internal standard used in the assays was the $^{6}C_{13}$ analog of GDC-0973.

PK Analysis. PK parameters were calculated by noncompartmental methods as described in Gibaldi and Perrier (1982) using WinNonlin (Pharsight, Mountain View, CA) version 5.1.1. Parameters are presented as mean ± S.D. Bioavailability (F) was determined by dividing the dose-normalized area under the plasma concentration-time curve from time 0 extrapolated to infinity (AUC_{inf}) for each animal dosed orally by the dose-normalized mean AUC_{inf} determined from the animals dosed intravenously (a pooled profile was used in mice).

Determination of pERK Inhibition in Mouse Brain. To test whether MEK pathway inhibition (as measured by pERK inhibition) was observed in the brain at efficacious doses, brain tissue from mice was collected and prepared for Western blotting using methods described previously (Choo et al., 2010). Antibodies to pERK and total ERK proteins were obtained from Cell Signaling Technology (Danvers, MA). Specific antigen-antibody interaction was detected with a horseradish peroxidase-conjugated secondary antibody IgG using enhanced chemiluminescence Western blotting detection reagents (GE Healthcare, Chalfont St. Giles, Buckinghamshire, UK).

Quantitative Whole-Body Autoradiography in Rat. The tissue distribution of [^{14}C]GDC-0973-related radioactivity in male Long-Evans rats (Harlan, Scottsdale, PA) was investigated after a single oral dose of 30 mg/kg (100 μCi/kg) [^{14}C]GDC-0973 (Ricera BioScience LLC, Concord, OH) combined with GDC-0973 formulated in MCT. One animal was euthanized under isoflurane anesthesia at 0.5, 2, 4, 8, 24, 72, 96, 240, 480, and 672 h postdose. The carcasses were frozen in hexane dry ice and stored at −20°C before processing for quantitative whole-body autoradiography (QWBA). Before section collection, standards fortified with ^{14}C radioactivity were placed into the frozen block containing the carcass. Each carcass was embedded, cut into sagittal sections, and mounted for QWBA. Selected sections were exposed to phosphor image screens, and exposed screens were scanned along with plastic-embedded ARC autoradiographic standards (American Radiolabeled Chemicals, Inc., St Louis, MO) for subsequent calibration of the image analysis software. Screens were exposed for 4 days, after which they were scanned using a Storm Scanner (GE Healthcare Life Sciences, Sunnyvale, CA). Tissue radioactivity concentrations were quantified from the whole-body autoradiograms using Imaging Research AIS software (Imaging Research, St. Catharines, ON, Canada) on the basis of a calibrated standard curve. Concentrations of radioactivity were expressed as microcuries per gram and were converted to microgram equivalents of GDC-0973 per gram of matrix using the specific activity (55 mCi/mmol) of the administered dose of [^{14}C]GDC-0973, which was a combination of radiolabeled and nonradiolabeled compound.

Mass Balance and Routes of Elimination in Rat. A single dose of [^{14}C]GDC-0973 (30 mg/kg, 400 μCi/kg; Ricera Bioscience LLC) was administered orally to bile duct-intact ($n = 3$ male and 3 female) and bile duct-cannulated (BDC) male ($n = 3$) Sprague-Dawley rats (QPS LLC, Newark, DE). The dose was prepared MCT. Urine and feces were collected in plastic containers surrounded by dry ice at predose (overnight for at least 12 h) and 0 to 8 and 8 to 24 h postdose, and at 24-h intervals through 48 (BDC rats) or 192 h (intact rats) postdose. Bile was collected from BDC animals in plastic containers surrounded by dry ice at predose and 0 to 8, 8 to 24, and 24 to 48 h postdose. Blood (approximately 0.5 ml) was collected from a jugular vein via syringe and needle and was transferred into tubes containing K_2EDTA as the anticoagulant at predose and at 0.5, 1, 2, 4, 8, 24, and 48 h postdose. All samples were stored at approximately −70°C before and after analysis. Blood was stored at approximately 4°C until centrifuged. Plasma was harvested, aliquoted, and stored at approximately −70°C. Feces or feces homogenate was combusted using a model 307 Sample Oxidizer (PerkinElmer, Downers Grove, IL), and the resulting $^{14}CO_2$ was trapped in a mixture of Perma-Fluor and Carbo-Sorb (PerkinElmer). Ultima Gold XR scintillation cocktail was added to all other samples and was analyzed directly. Samples were analyzed in duplicate or triplicate (feces). Radioactivity content was quantified by liquid scintillation counting [model 2800TR liquid scintillation counters (PerkinElmer)] for at least 5 min or 100,000 counts.

Mass Balance and Routes of Elimination in Dog. A single dose of [^{14}C]GDC-0973 (5 mg/kg, 20 μCi/kg; Ricera Bioscience LLC) was administered orally to bile duct-intact ($n = 2$ male and 2 female) and BDC male ($n = 2$) Beagle dogs (Covance Laboratories). The dose was prepared in MCT. Urine and feces were collected in plastic containers surrounded by dry ice at predose (overnight for at least 12 h) and at 0 to 8 and 8 to 24 h postdose, and at 24-h intervals through 168 (BDC dogs) or 240 h (intact dogs) postdose. Bile was collected from BDC animals into plastic containers surrounded by dry ice predose at 0 to 8, 8 to 24, and at 24-h intervals through 168 h postdose. Blood (approximately 5 ml) was collected from intact dogs from a jugular vein via syringe and needle and was transferred into tubes containing K_2EDTA as the anticoagulant at predose and at 0.083, 0.25, 0.5, 1, 3, 6, 12, 24, 48, 72, 96, 120, 168, and 240 h postdose in both intact and BDC dogs. All samples were stored, prepared, and analyzed as described for the rat mass balance study above.

Colo205 Xenograft Efficacy Studies. Five million human colorectal carcinoma Colo205 cells were resuspended in Hanks' buffered salt solution and were implanted subcutaneously into the right flank of naive female athymic nu/nu mice. Tumors were monitored until they reached a mean volume of 200 to 300 mm^3. Tumor sizes and body weights were recorded twice weekly, and the mice were observed regularly over the course of the study. Mice were

euthanized if their tumor volume exceeded 2000 mm^3 or if their body weight dropped by more than 20% of the starting weight. Ten mice were randomly assigned to each group on the basis of mean tumor volume. Mean tumor volume across all six groups was 200 mm^3 at the start of dosing. Tumor volumes were measured in two dimensions (length and width) using Ultra Cal-IV calipers (model 54-10-111; Fred V. Fowler Company, Inc., Newton, MA). The following formula was used with Excel version 11.2 (Microsoft Corporation, Redmond, WA) to calculate tumor volume (TV): TV (mm^3) = (length × width^2) × 0.5.

GDC-0973 or vehicle was administered daily (at a similar time of the day) by oral gavage for 20 days or until animals lost >20% of body weight or until tumor size was >2000 mm^3. Animals in vehicle groups received 100 μl of MCT. Treatment groups (n = 10 mice/group) received oral doses of GDC-0973 formulated in 100 μl of MCT. The treatment groups were as follows: vehicle, 1, 3, 10, and 30 mg/kg.

PK-Pharmacodynamic Modeling. Fitting of the PK-pharmacodynamic (PD) model to the efficacy data and mouse PK were performed using SAAM II (Saam Institute, University of Washington, Seattle, WA).

An indirect response model (Mager et al., 2003) was used to fit the xenograft efficacy data; the differential equation is as follows:

$$\frac{d(\mathrm{TV})}{\mathrm{dt}} = k_{ng}(\mathrm{TV}) - K(\mathrm{TV})$$

where

$$K = \frac{\mathrm{K}_{max} \times C^n}{\mathrm{KC}_{50}{}^n + C^n}$$

TV (mm^3) is defined as the tumor volume, t (h) is time, k_{ng} (h^{-1}) is the net growth rate constant, K (h^{-1}) is the rate constant describing the tumor growth inhibition (TGI) effects of GDC-0973, K_{max} (h^{-1}) is the maximal value of K, C (μM) is the concentration of GDC-0973, n is the Hill coefficient, and KC_{50} (μM) is the GDC-0973 concentration where K is 50% of K_{max}. Concentrations of GDC-0973 in mice were simulated on the basis of parameters obtained from fitting the time-concentration data from PK studies. Mean tumor volumes for each dose group were used in the fitting. All dose groups were fit simultaneously. PD parameters are presented as the estimate followed by the percentage CV in parentheses. Concentration required for tumor stasis (C_{stasis}) was calculated as the concentration where K is equal to k_{ng}.

Prediction of Human PK Parameters and Efficacious Doses. Prediction of human CL and volume of distribution for GDC-0973 was performed prospectively by allometric scaling on the basis of the equation CL = aW^b, where a, W, and b are the allometric coefficient, body weight, and allometric exponent, respectively (Boxenbaum, 1982). Total plasma CL and volume of distribution values obtained from PK studies in preclinical species were scaled on the basis of body weight to predict the systemic CL and volume of distribution in human. Body weights of 0.02, 0.25, 10, 3, and 70 kg were used for mouse, rat, dog, monkeys, and human, respectively. The human dose associated with 90% TGI was simulated on the basis of parameter estimates from PK-PD modeling of Colo205 xenografts in mouse and by substituting human predicted PK parameters for mouse PK estimates.

Results

Permeability in MDCK and MDR1-MDCK Cells. GDC-0973 mean P_{app} (n = 8) in MDCK cells was moderate with A-B values of 1.39 ± 0.271 10^{-6} cm/s and B-A values of 4.00 ± 0.215 10^{-6} cm/s. The ER was low at ~3.0, suggesting minor involvement of efflux transporter(s) in the B-A direction in this cell line. In the MDR1-transfected MDCK cell line, the A-B value was 0.88 ± 0.05 and the B-A ratio was 35.4 ± 6.0 10^{-6} cm/s, with a mean ER of 40, confirming the involvement of MDR1. Cyclosporine (25 μM) was able to increase the A-B ratio to 2.57 ± 0.45 10^{-6} cm/s and decrease the ER to 1.6. In comparison, for digoxin (the positive control), the ER was 72. These data suggest that GDC-0973 appears to be a substrate of MDR1. In this assay, GDC-0973 (25 μM) did not appear to be an inhibitor of MDR1 (based on inhibition of digoxin efflux; data not shown).

In Vitro Protein Binding and Blood-to-Plasma Partitioning. Plasma protein binding was determined by equilibrium dialysis at GDC-0973 concentrations of 1, 5, and 10 μM in mouse, rat, cynomolgus monkey, dog, and human pooled plasma. GDC-0973 was highly bound to plasma protein, with the highest percentage of unbound GDC-0973 varying approximately 10-fold between species (Table 1).

GDC-0973 appeared to be more highly bound to α-1-acid glycoprotein (AAG) compared with albumin. Protein binding across species was independent of concentration (1–10 μM). The free fraction of GDC-0973 in mouse brain homogenates was determined to be 0.12%.

Blood-to-plasma partitioning of GDC-0973 was evaluated in mouse, rat, cynomolgus monkey, dog, and human pooled whole blood at concentrations of 1, 5, and 10 μM. Mean blood-to-plasma ratios ranged from 0.623 to 1.51 in all species tested and were independent of concentration (Table 2). Thus, GDC-0973 shows no substantial binding to red blood cell components.

Metabolic Stability Study in Liver Microsomes. The predicted hepatic CL of GDC-0973 from the metabolic stability after a 1-h incubation in liver microsomes in mouse, rat, dog, monkey, and human was 45, 30, 14, 34, and 10 ml · min^{-1} · kg^{-1}, respectively. Except for dog, the predicted CL was generally well predicted by microsomes.

Pharmacokinetics of GDC-0973 in Mouse, Rat, Cynomolgus Monkey, and Dog. The semilog plots of GDC-0973 plasma concentration versus time for mouse, rat, monkey, and dog after intravenous and oral administrations are presented in Fig. 2. The PK parameters are presented in Table 3. Total blood CL for all species was in the moderate range (relative to liver blood flow) (Davies and Morris, 1993). Terminal half-life values ranged from approximately 4 h in the mouse to 13 h in the rat. The volume of distribution at steady state (V_{ss}) was moderate to high in all species evaluated. After oral administration, bioavailability ranged from 20 in monkey to 93% in mouse.

TABLE 1

Mean (±S.D.) percentage of [^{14}C]GDC-0973 bound in mouse, rat, dog, cynomolgus monkey, human plasma, human AAG, and HSA

Matrix/Species	Total GDC-0973 Concentration[a]	Percentage Unbound [^{14}C]GDC-0973
	μM	
Mouse	1	4.1 ± 0.8
	5	3.4 ± 0.1
	10	3.3 ± 0.2
Rat	1	2.8 ± 0.4
	5	3.5 ± 0.4
	10	3.7 ± 0.3
Dog	1	0.7 ± 0.0
	5	1.2 ± 0.2
	10	1.4 ± 0.2
Cynomolgus monkey	1	4.5 ± 1.1
	5	4.4 ± 0.3
	10	4.8 ± 0.3
Human	1	5.2 ± 0.4
	5	6.5 ± 0.4
	10	5.8 ± 0.2
AAG, 1 mg/ml	1	4.4 ± 0.6
	5	4.2 ± 0.2
	10	5.3 ± 0.1
HSA, 40 mg/ml	1	46.9 ± 14.9
	5	40.8 ± 0.2
	10	40.8 ± 1.2

[a] Unlabeled + [^{14}C]-labeled GDC-0973 (free-base equivalents).

TABLE 2

Mean (±S.D.) blood-to-plasma ratio of [^{14}C]GDC-0973 in mouse, rat, dog, cynomolgus monkey, and human whole blood

Species	Total GDC-0973 Concentration[a]	Blood-to-Plasma Ratio of [^{14}C]GDC-0973
	μM	
Mouse	1	1.16 ± 0.03
	5	1.19 ± 0.03
	10	1.27 ± 0.02
Rat	1	1.36 ± 0.02
	5	1.37 ± 0.02
	10	1.51 ± 0.08
Dog	1	0.632 ± 0.011
	5	0.752 ± 0.009
	10	0.936 ± 0.011
Cynomolgus monkey	1	1.57 ± 0.04
	5	1.64 ± 0.03
	10	1.82 ± 0.07
Human	1	0.933 ± 0.014
	5	0.945 ± 0.007
	10	1.05 ± 0.01

[a] Unlabeled + [^{14}C]-labeled GDC-0973 (free-base equivalents).

Determination of GDC-0973 Concentrations and pERK Inhibition in Mouse Brain. Taking into account the free fraction of GDC-0973 in mouse brain (fu 0.0012), the unbound AUC of GDC-0973 was low, 0.003 μM · h. The low concentration of GDC-0973 in the brain is consistent with the lack of pERK inhibition observed in the brain (Fig. 3B). This is in comparison with the pERK knockdown observed with the positive control. In a separate study, at the 2-h time point, the brain unbound concentrations at the 3 mg/kg dose was 0.0001 μM, and the unbound plasma concentration was 0.0057 μM, resulting in a unbound brain-to-plasma ratio of 0.018 (total brain-to-plasma ratio ~0.5). The low penetration of GDC-0973 into the brain suggests that GDC-0973 is effluxed out of the brain. Interestingly, the total tumor (Colo205) concentration of GDC-0973 at the 2-h time point was 1.56 μM (total tumor-to-plasma ratio ~9), suggesting that GDC-0973 accumulates in tumors.

Quantitative Whole-Body Autoradiography in Rat. After oral administration of ^{14}[C]GDC-0973 (30 mg/kg), compound related radioactivity in tissue was observed by 2 h post dose with extensive distribution into tissues and organs (Fig. 3A). The tissues showing the highest peak concentrations were the liver, large intestine, lungs, adrenal glands and lacrimal glands. Radioactivity in the central nervous system e.g., the cerebrum were low and were below the levels of detection by 4 h postdose. By 72 h, in most tissues, radioactivity levels were below the limit of detection with the exception for the organs of elimination e.g., liver, kidney intestine, as well as melanin containing tissue.

Mass Balance and Routes of Elimination in Rat. The excretion of radioactivity was determined after administration of a single oral dose of [^{14}C]GDC-0973 (30 mg/kg) to bile duct-intact and BDC male and female Sprague-Dawley rats. [^{14}C]GDC-0973-related radioactivity was rapidly excreted after oral administration to bile duct-intact male and female rats, primarily within the first 48 h after dosing (~80% excreted). Routes and rates of excretion were similar in both males and females (Fig. 4, A and B). A high percentage of radioactivity was recovered in feces (~85%), and only 2.2 to 4.4% of radioactivity was recovered in urine (Fig. 4A). Approximately 74 to 81% of the administered radioactivity was recovered in the bile of BDC rats through 48 h postdose (Fig. 4B), with low amounts of radioactivity in feces. The combined recovery in urine and bile indicated that approximately 80% of the oral dose was absorbed in male and female BDC rats.

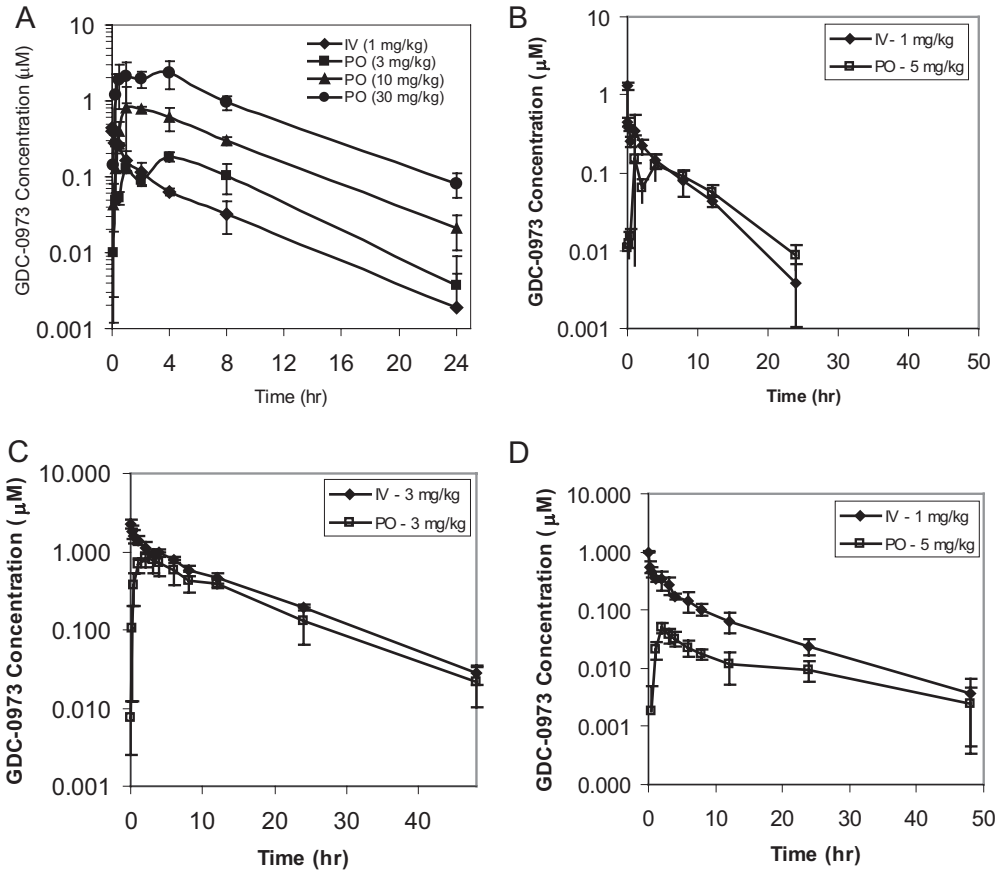

FIG. 2. Plasma concentration of GDC-0973 in nu/nu mouse (A), rat (B), dog (C), and monkey (D) after intravenous and oral administration.

TABLE 3

Pharmacokinetics (mean ± S.D.) of GDC-0973 after single-dose intravenous and oral administration to mouse, rats, dogs, and monkeys

Parameters	Nude Mice	Sprague-Dawley Rats	Beagle Dogs	Cynomolgus Monkeys
Sex	Female	Male	Male	Male
Intravenous				
Dose, mg/kg	1	3	3	3
Plasma CL, ml · min^{-1} · kg^{-1}	33.5	37.8 ± 7.2	5.53 ± 0.31	29.6 ± 8.5
AUC_{inf}, ng · h/ml	0.935	2.32 ± 0.18	17.1 ± 1.0	3.34 ± 0.87
$t_{1/2}$, h	3.92	13.3 ± 2.5	9.19 ± 1.57	10.3 ± 3.3
V_{ss}, l/kg	9.40	34.6 ± 8.5	3.99 ± 0.58	29.6 ± 8.5
Oral				
Dose, mg/kg	3	3	3	3
AUC_{inf}, ng · h/ml	1.51	1.59 ± 0.10	11.9 ± 2.6	0.64 ± 0.12
C_{max}, ng/ml	0.184	0.193 ± 0.125	0.843 ± 0.214	0.050 ± 0.010
T_{max}, h	0.250	3.50	2.67	2.00
F, %	53.9	69.0 ± 8.0	69.1 ± 11.7	19.6 ± 3.5

Mass Balance and Routes of Elimination in Dog. The excretion of radioactivity was determined after administration of a single oral dose of [^{14}C]GDC-0973 (5 mg/kg) to bile duct-intact and BDC male and female Beagle dogs. Approximately 80% of [^{14}C]GDC-0973-derived radioactivity was excreted after oral administration to dogs within the first 72 h after dosing. Routes and rates of excretion were similar in both males and females (Fig. 4C). A high percentage of radioactivity was recovered in feces (~80%), and only 6.3 to 7.0% of radioactivity was recovered in urine (Fig. 4C). Approximately 65% of the administered radioactivity was recovered in the bile of BDC dogs through 168 h postdose (Fig. 4C), with a low amount of radioactivity recovered in feces. The combined recovery in urine and bile indicated that approximately 70% of the oral dose was absorbed in BDC dogs.

In Vivo Xenograft Potency Assessment. TGI curves after a range of oral doses of GDC-0973 in Colo205 (BRAF V600E mutant) xenograft tumor-bearing mice are shown in Fig. 5A. Overall, GDC-0973 showed dose-dependent inhibition of tumor growth up to a dose of 10 mg/kg with saturation of efficacy observed at the highest dose tested (30 mg/kg). Figure 5B compares observed and predicted tumor volumes after simultaneous fitting of a simple indirect response model to the Colo205 tumor data (eq. 1). In general, a simple indirect response model was able to adequately characterize the PK-PD relationship between GDC-0973 plasma concentrations and TGI. Estimated in vivo GDC-0973 PD parameters (%CV) characterizing the relationship were as follows: KC_{50} = 0.389 μM (21) (207 ng/ml; total concentration), K_{max} = 0.0326 h^{-1} (14), k_{ng} = 0.00372 h^{-1} (3), and n = 1 (fixed). Total concentration required for tumor stasis (C_{stasis}) was 0.05 μM (the concentration where the K is equal to k_{ng}).

Human PK and Dose Predictions. On the basis of allometry with maximal life-span potential (MLP) correction for CL (exponent >0.7), the correlation coefficient of the linear regression of log CL or volume of distribution (across species) versus log body weight was 0.94 and 0.85 for CL and volume of distribution, respectively. A total human plasma CL and volume of distribution of 2.9 ml · min^{-1} · kg^{-1} and 9.9 l/kg, respectively, were predicted on the basis of the following regressions: CL × MLP = 2.23W$^{1.11}$ and volume of distribution = 1.13W$^{0.93}$. Because the current literature does not suggest that accounting for protein binding increases the accuracy in predicting human CL (Mahmood, 2005), the dose predictions were based on total CL. Assuming a one-compartment PK model, the predicted CL, volume of distribution, half-life (k_e = 0.0176 h^{-1}; $t_{1/2}$ ~ 39 h), an absorption rate constant (k_a) of 1.00 h^{-1} (on the basis of the k_a from fitting the dog PK data), and an assumed bioavailability of 80%, an estimate of a human PK profile was predicted. The predicted human dose (based on predicted PK) associated with the 90% TGI (compared with vehicle) at the end of study based on estimates from fitting the data from the Colo205 model was determined to be approximately 10 mg, dosed daily. The predicted human PK profiles associated with a 10-mg dose based on a one-compartment model are shown in Fig. 5C [area under the curve (AUC) and C_{max} of ~655 ng · h/ml and ~11 ng/ml, $t_{1/2}$ ~ 39 h].

Discussion

Identification of potent and efficacious MEK inhibitors has been an active area of research. Currently, there are numerous MEK inhibitors at various stages of oncology clinical development (Frémin and Meloche,

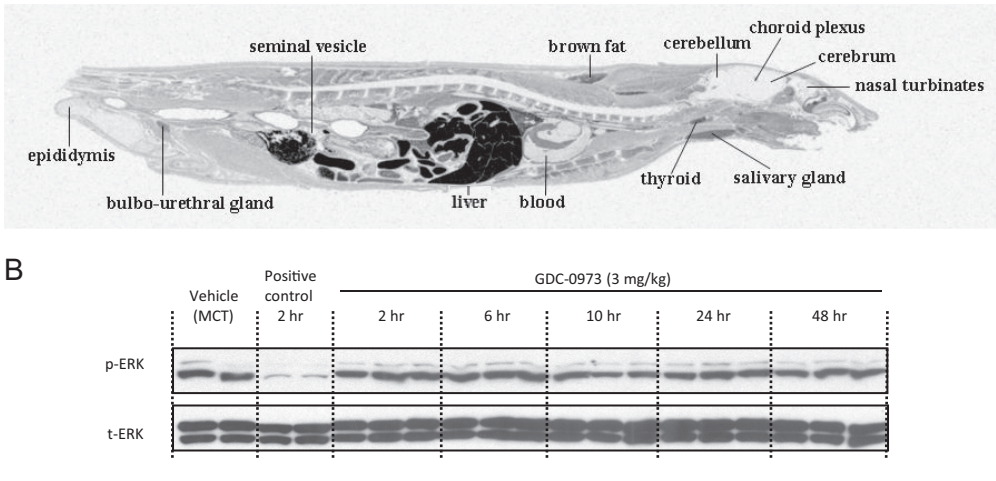

FIG. 3. A, whole-body autoradiogram of GDC-0973-related radioactivity distribution in male Long-Evans rat at 2 h after a single administration of 30 mg/kg [^{14}C]GDC-0973. B, pERK in the brain of mice after the fifth daily dose of 3 mg/kg GDC-0973.

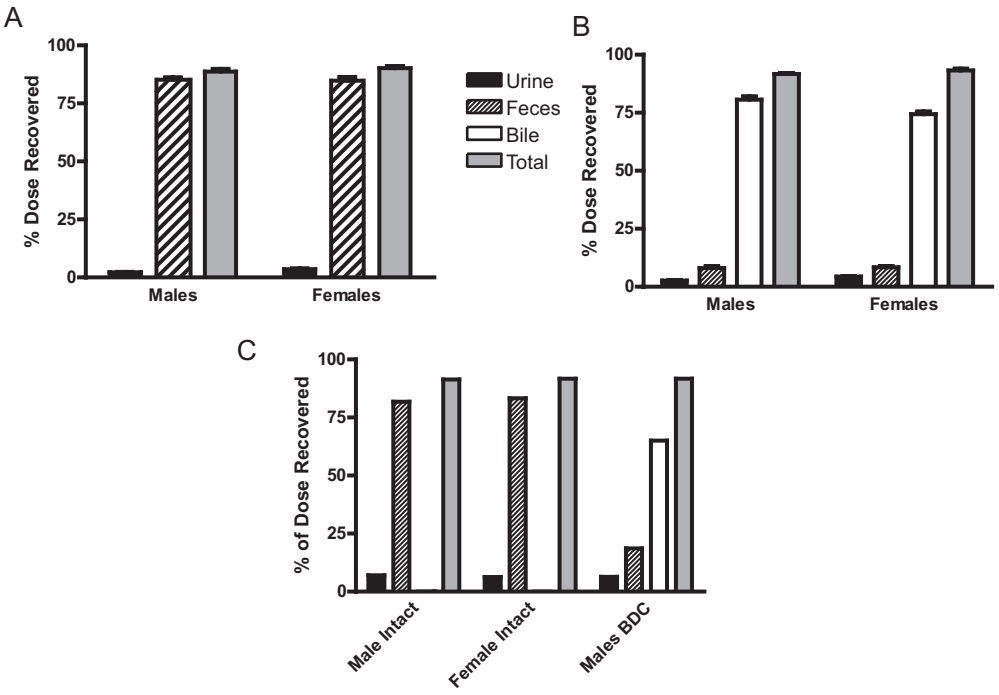

FIG. 4. Recovery of [^{14}C]GDC-0973-related radioactivity after oral administration of 30 mg/kg to male and female bile duct intact rats (A) and bile duct cannulated rats (B). Recovery of [^{14}C]GDC-0973-related radioactivity after oral administration of 5 mg/kg to male and female bile duct intact dogs and bile duct cannulated male dogs (C).

2010). Signs of clinical activity have been reported for GDC-0973 (Rosen et al., 2011) and GSK1120212 (Gilmartin et al., 2011) in Phase Ib trials in melanoma tumors bearing the BRAF V600E mutation. In addition, the BRAF inhibitor, vemurafenib, which acts downstream of MEK, has shown efficacy in the treatment of BRAF V600E melanoma (Flaherty et al., 2009; Puzanov et al., 2009; Bollag et al., 2010) and has been approved for treatment of BRAF mutant melanoma.

Before clinical development of a compound, as part of the discovery process, preclinical assessment is conducted to understand the absorption, distribution, metabolism, and excretion of the compound. In addition, preclinical efficacy is also assessed and exposure-efficacy relationships are characterized. Collectively, this information forms the basis for predicting the human disposition, efficacy, and target dose of a compound in humans. Finally, when clinical information

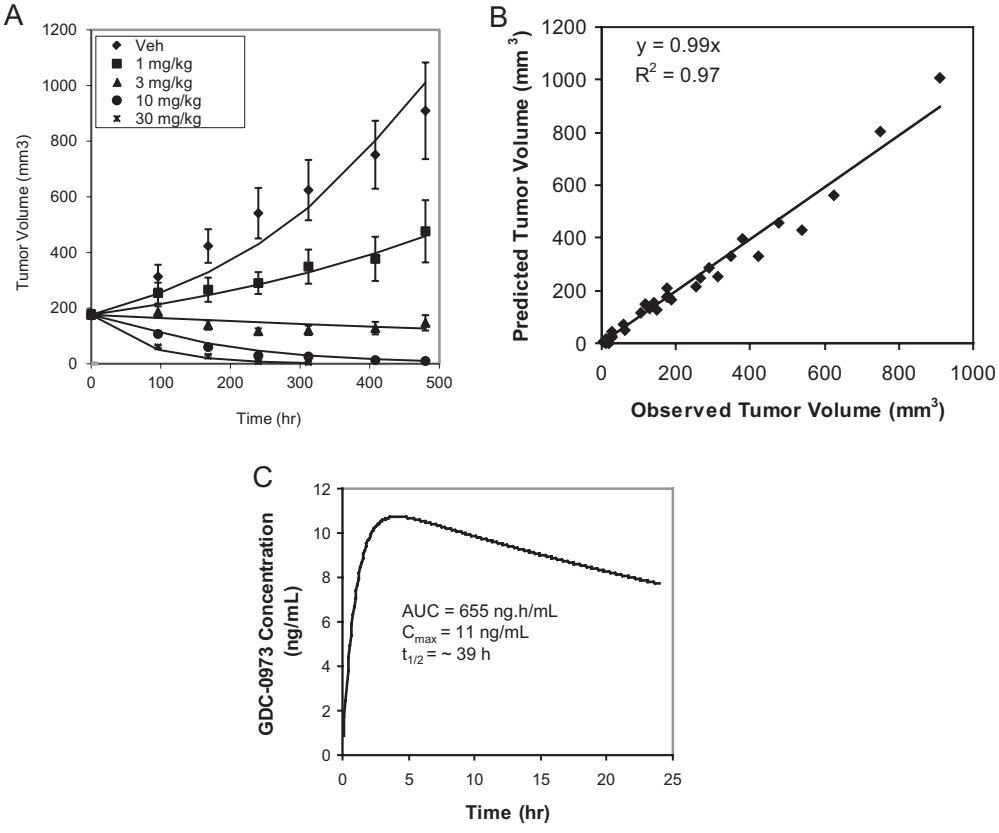

FIG. 5. Effect of GDC-0973 administration on the growth of Colo205 tumor xenografts in mice. Tumor volumes are presented as mean ± S.E. (symbols, observed data; line, fit of indirect response model to data) (A). Observed versus predicted tumor volumes after fit of an indirect response model to the data (B). Simulated concentration-time profile of 10 mg of GDC-0973 (concentration predicted to be associated with 90% TGI in the Colo205 xenograft model; predicted CL of 2.9 ml · min^{-1} · kg^{-1}, V_{ss} of 9.9 l/kg, and assumed F of 80%) (C).

becomes available, it is important to retrospectively revisit earlier predictions to learn and confirm from previous experiences.

GDC-0973 is characterized to have high protein binding across species (~1–6% unbound). Data from the rat QWBA study suggest that GDC-0973 is distributed rapidly and extensively into tissues. In the QWBA study, the highest concentration of compound-related radioactivity was observed in liver and bile, persisting beyond measurable levels in blood. This is consistent with data from the mass balance studies showing that in both rat and dog, biliary excretion is the major pathway for GDC-0973 elimination, with renal excretion playing a minor role. In addition, the QWBA data show low levels of GDC-0973-related radioactivity in the brain (Fig. 3), similar to data indicating that GDC-0973 does not appear to penetrate the brain appreciably. In addition, pERK inhibition, a downstream biomarker for MEK pathway inhibition, was not observed in brain tissue. The low unbound brain-to-plasma ratio (0.018) at 2 h suggests that the disproportionately low concentrations in brain may be limited by efflux. This is in keeping with studies in MDCK cells overexpressing P-gp, suggesting that GDC-0973 is a substrate for P-gp. However, unlike in brain, levels of GDC-0973 in Colo205 tumors were greater than plasma concentrations, suggesting lack of P-gp influence/expression in Colo205 xenograft tumors.

In preclinical species, the PK of GDC-0973 is characterized by moderate CL across species and a large volume of distribution. There are numerous methods that could be employed in CL predictions (Poulin et al., 2011a; Ring et al., 2011). In the case of GDC-0973, we chose to use allometry using all available preclinical CL data (with MLP correction based on the exponent) for scaling total CL. On the basis of allometry, the plasma CL in human was predicted to be low (~3 ml · min^{-1} · kg^{-1}); this is lower than the predicted CL (10 ml · min^{-1} · kg^{-1}) based on microsomes. On the basis of allometry, the volume of distribution was predicted to be high (~10 l/kg), with a predicted half-life of 39 h. The assumed F was 80%, which is consistent with the moderate permeability observed in MDCKI cell lines, the F observed in preclinical species (except monkey), the high fraction absorbed observed in the mass balance studies in rat and dog, and the predicted CL ($F = 1 - E$; assuming total CL is hepatic). Assuming a one-compartment model, the predicted CL of 3 ml · min^{-1} · kg^{-1}, V_{ss}, and F, a 10-mg dose of GDC-0973 is associated with an AUC and C_{max} of ~655 ng · h/ml and ~11 ng/ml (T_{max} ~4 h) (Fig. 5).

It has been reported that the clinically observed half-life of GDC-0973 ranges from 26 to 53 h (Musib et al., 2011), similar to the predicted half-life of 39 h. At a 10-mg dose in the clinic, the observed AUC and C_{max} were 752 ng · h/ml and 53 ng/ml (T_{max} ~ 4 h), respectively (Musib et al., 2011). Therefore, overall, the AUC of GDC-0973 was well predicted. However, the discrepancy (~5-fold) between the predicted and observed C_{max} may be explained in part by the PK profile of GDC-0973, which was described by a two-compartment model with an absorption lag time (Budha et al., 2011), whereas a one-compartment model and absorption rate constant from dog was applied in the predictions. It is often difficult a priori to predict the PK profile of compounds, particularly if the profile is described by multiple compartments. Alternative methods proposed by Dedrick et al. (1970) or Wajima et al. (2004) and physiology-based PK modeling have been used to project human concentration-time profiles. However, according to other studies, prediction of PK profiles of orally dosed compounds was relatively poor using these methods (Poulin et al., 2011b; Vuppugalla et al., 2011), highlighting the continuing challenge in predicting oral concentration-time profiles.

Interestingly, the KC_{50} (16 nM; unbound plasma), describing the in vivo potency, was consistent with the IC_{50} values from the enzyme (4.2), cellular pERK (1.8), and proliferation (8 nM) assays in Colo205 cells. The predicted efficacious dose in humans was determined on the basis of PK-PD modeling of the Colo205 (V600E mutant) mouse xenograft efficacy data. Estimates from this modeling were used to simulate human doses associated with 90% TGI (compared with vehicle) in human by substituting mouse PK for predicted human PK, thereby accounting for the difference in mouse PK and human predicted PK. According to the Colo205 model, a ~10-mg daily dose of GDC-0973 is associated with 90% TGI. It has been reported that clinical signs of efficacy have been observed with GDC-0973 in BRAF V600E melanoma patients at doses of 60 and 100 mg, dosed daily for 21 and 14 days, respectively, in a 28-day cycle of treatment (Rosen et al., 2011). Considering the difference between the predicted and observed human PK, these data suggest the Colo205 model appears to be a sensitive model and underestimated the clinical efficacious dose of GDC-0973 because activity was observed at higher doses (60 mg) than predicted (~10 mg). Preliminary data suggest that clinical efficacy is observed at doses where efficacy is saturated in the Colo205 model. However, according to the H2122 (KRAS, non–small-cell lung cancer) and A2058 (BRAF mutant, PTEN-null model) xenograft data, higher doses are predicted to be required for efficacy (data not shown), suggesting that less sensitive in vivo models may provide a better prediction of the ultimate clinical efficacious dose. Because signs of clinical efficacy are observed in melanoma patients with the BRAF V600E mutation, the Colo205 (V600E) xenograft model appears to be the relevant genotype for comparison. Because prospectively we do not necessarily know the responsive tumor type(s) in the clinic, it highlights the importance for assessing multiple models with varying sensitivity in predicting a clinical efficacious dose.

It is also interesting to note that in the Colo205 xenograft model, vemurafenib has been reported to show tumor stasis and regression at exposures (AUC) between 200 and 300 μM · h in the mouse (Bollag et al., 2010), whereas the clinical dose (960 mg b.i.d.) is associated with an AUC of 1741 μM · h (Flaherty et al., 2010). This suggests that as with GDC-0973, higher exposures of vemurafenib were required clinically compared with preclinical estimates based on the Colo205 xenograft model. It is also interesting to note that the administration of the MEK inhibitor, GSK1120212 is associated with 85 and 83% TGI at a dose of 3 mg/kg in the Colo205 and HCT116 (KRAS mutant) xenograft model, respectively (Gilmartin et al., 2011). However, because mouse exposures are not reported, comparisons of mouse exposures with human exposures at 2 mg (recommended Phase II dose; AUC 360 ng · h/ml) where signs of efficacy have been observed cannot be made (Infante, et al., 2010).

There are multiple caveats in translating preclinical efficacy data to human efficacy predictions. One primary assumption is that concentrations required for antitumor activity translate directly from mouse xenograft models to humans. This assumes that distribution of drug is similar despite reported differences in tumor vasculature and transport in xenograft versus human tumors (Jang et al., 2003). Another assumption is that the capacity (E_{max}) and sensitivity (EC_{50}) parameters are conserved across species (Mager et al., 2009). In addition, noted differences in growth rate and previous exposure of human tumors to prior therapies may complicate the interpretation of modeled xenograft data. Nevertheless, despite these limitations, there have been numerous reports where preclinical PK-PD modeling has been successfully applied in predicting dose targets associated with human efficacy (Simeoni et al., 2004; Tanaka et al., 2008; Rocchetti et al., 2009; Goteti et al., 2010).

Drug discovery and development is an iterative process. As compounds progress in the clinic, it is important to apply the "learn and

confirm" paradigm. Here, with GDC-0973, where possible we have revisited and compared the preclinical data and predictions with observed clinical data. It is hoped that by learning from examples such as GDC-0973, this may ultimately lead to a more successful drug discovery/development process.

Acknowledgments

We thank Genentech colleagues in the Translational Oncology and Drug Metabolism and Pharmacokinetics departments. We also thank the In Vivo Studies Group for contributions in generating data for this study.

Authorship Contributions

Participated in research design: Choo, Belvin, Hoeflich, Merchant, Plise, Robarge, Martini, Aoyama, Ramaiya, and Johnston.

Conducted experiments: Orr and Plise.

Contributed new reagents or analytic tools: Deng and Robarge.

Performed data analysis: Boggs, Ly, Plise, Kassees, and Ramaiya.

Wrote or contributed to the writing of the manuscript: Choo.

References

Belvin M, Berry L, Chan J, den Otter D, Friedman L, Hoeflich K, Koeppen H, Merchant M, Orr C, and Rice K (2010) Intermittent dosing of the MEK inhibitor, GDC-0973, and the PI3K inhibitor, GDC-0941, results in prolonged accumulation of Bim and causes strong tumor growth inhibition in vivo. *22nd EORTC–NCI–AACR Symposium on Molecular Targets and Cancer Therapeutics Programme*; 2010 Nov 16–19; Berlin, Germany. European Organization for Research and Treatment of Cancer, Brussels, Belgium.

Bollag G, Hirth P, Tsai J, Zhang J, Ibrahim PN, Cho H, Spevak W, Zhang C, Zhang Y, Habets G, et al. (2010) Clinical efficacy of a RAF inhibitor needs broad target blockade in BRAF-mutant melanoma. *Nature* **467:**596–599.

Boxenbaum H (1982) Interspecies scaling, allometry, physiological time, and the ground plan of pharmacokinetics. *J Pharmacokinet Biopharm* **10:**201–227.

Budha N, Jin J, Musib L, Eppler S, Ware J, Chan I, and Dresser M (2011) Population pharmacokinetics of MAPK kinase (MEK) inhibitor GDC-0973 in phase I patients with solid tumors. *American Society of Clinical Pharmacology and Therapeutics Annual Meeting*; 2011 Mar 3; Dallas, TX. American Society of Clinical Pharmacology and Therapeutics, Alexandria, VA.

Choo EF, Belvin M, Chan J, Hoeflich K, Orr C, Robarge K, Yang X, Zak M, and Boggs J (2010) Preclinical disposition and pharmacokinetics-pharmacodynamic modeling of biomarker response and tumour growth inhibition in xenograft mouse models of G-573, a MEK inhibitor. *Xenobiotica* **40:**751–762.

Choo EF, Driscoll JP, Feng J, Liederer B, Plise E, Randolph N, Shin Y, Wong S, and Ran Y (2009) Disposition of GDC-0879, a B-RAF kinase inhibitor in preclinical species. *Xenobiotica* **39:**700–709.

Davies B and Morris T (1993) Physiological parameters in laboratory animals and humans. *Pharm Res* **10:**1093–1095.

Dedrick R, Bischoff KB, and Zaharko DS (1970) Interspecies correlation of plasma concentration history of methotrexate (NSC-740). *Cancer Chemother Rep* **54:**95–101.

Downward J (2003) Targeting RAS signalling pathways in cancer therapy. *Nat Rev Cancer* **3:**11–22.

Flaherty K, Puzanov I, Sosman J, Kim K, Ribas A, McArthur G, Lee RJ, Grippo JF, Nolop K, and Chapman P (2009) Phase I study of PLX4032: proof of concept for V600E BRAF mutation as a therapeutic target in human cancer. *J Clin Oncol* **27:**15s.

Flaherty KT, Puzanov I, Kim KB, Ribas A, McArthur GA, Sosman JA, O'Dwyer PJ, Lee RJ, Grippo JF, Nolop K, et al. (2010) Inhibition of mutated, activated BRAF in metastatic melanoma. *N Engl J Med* **363:**809–819.

Frémin C and Meloche S (2010) From basic research to clinical development of MEK1/2 inhibitors for cancer therapy. *J Hematol Oncol* **3:**8.

Gibaldi M and Perrier D (1982) *Pharmacokinetics*, Marcel Dekker, New York.

Gilmartin AG, Bleam MR, Groy A, Moss KG, Minthorn EA, Kulkarni SG, Rominger CM, Erskine S, Fisher KE, Yang J, et al. (2011) GSK1120212 (JTP-74057) is an inhibitor of MEK activity and activation with favorable pharmacokinetic properties for sustained in vivo pathway inhibition. *Clin Cancer Res* **17:**989–1000.

Goteti K, Garner CE, Utley L, Dai J, Ashwell S, Moustakas DT, Gönen M, Schwartz GK, Kern SE, Zabludoff S, et al. (2010) Preclinical pharmacokinetic/pharmacodynamic models to predict synergistic effects of co-administered anti-cancer agents. *Cancer Chemother Pharmacol* **66:**245–254.

Hoeflich KP, Jaiswal B, Davis DP, and Seshagiri S (2008) Inducible BRAF suppression models for melanoma tumorigenesis. *Methods Enzymol* **439:**25–38.

Hoeflich KP, O'Brien C, Boyd Z, Cavet G, Guerrero S, Jung K, Januario T, Savage H, Punnoose E, Truong T, et al. (2009) In vivo antitumor activity of MEK and phosphatidylinositol 3-kinase inhibitors in basal-like breast cancer models. *Clin Cancer Res* **15:**4649–4664.

Infante JR, Fecher LA, Nallapareddy S, Gordon MS, Flaherty KT, Cox DS, DeMarini DJ, Morris SR, Burris HA, and Messersmith WA (2010) Safety and efficacy results from the first-in-human study of the oral MEK 1/2 inhibitor GSK1120212. *2010 American Society of Clinical Oncology Annual Meeting*; 2010 Jun 4–8; Chicago, IL. Abstract 2503. American Society of Clinical Oncology, Alexandria, VA.

Jang SH, Wientjes MG, Lu D, and Au JL (2003) Drug delivery and transport to solid tumors. *Pharm Res* **20:**1337–1350.

Johnson GL and Lapadat R (2002) Mitogen-activated protein kinase pathways mediated by ERK, JNK, and p38 protein kinases. *Science* **298:**1911–1912.

Kalvass JC, Maurer TS, and Pollack GM (2007) Use of plasma and brain unbound fractions to assess the extent of brain distribution of 34 drugs: comparison of unbound concentration ratios to in vivo p-glycoprotein efflux ratios. *Drug Metab Dispos* **35:**660–666.

Mager DE, Woo S, and Jusko WJ (2009) Scaling pharmacodynamics from in vitro and preclinical animal studies to humans. *Drug Metab Pharmacokinet* **24:**16–24.

Mager DE, Wyska E, and Jusko WJ (2003) Diversity of mechanism-based pharmacodynamic models. *Drug Metab Dispos* **31:**510–518.

Mahmood I (2005) *Interspecies Pharmacokinetic Scaling*, Pine House Publishers, Rockville, Maryland.

Musib L, Eppler S, Choo E, Deng A, Miles D, Hsu B, Rosen L, Sikic B, LoRusso P, Ma W, et al. (2011) Clinical pharmacokinetics of GDC-0973, an oral MEK inhibitor, in cancer patients: data from a Phase 1 study (Abstract 1304). *Cancer Res* **71:**1304.

Obach RS, Baxter JG, Liston TE, Silber BM, Jones BC, MacIntyre F, Rance DJ, and Wastall P (1997) The prediction of human pharmacokinetic parameters from preclinical and in vitro metabolism data. *J Pharmacol Exp Ther* **283:**46–58.

Poulin P, Jones HM, Jones RD, Yates JW, Gibson CR, Chien JY, Ring BJ, Adkison KK, He H, Vuppugalla R, et al. (2011a) PhRMA CPCDC initiative on predictive models of human pharmacokinetics, part 1: goals, properties of the PhRMA dataset, and comparison with literature datasets. *J Pharm Sci* **100:**4050–4073.

Poulin P, Jones RD, Jones HM, Gibson CR, Rowland M, Chien JY, Ring BJ, Adkison KK, Ku MS, He H, et al. (2011b) PHRMA CPCDC initiative on predictive models of human pharmacokinetics, part 5: prediction of plasma concentration-time profiles in human by using the physiologically-based pharmacokinetic modeling approach. *J Pharm Sci* **100:**4127–4157.

Puzanov I, Nathanson KL, Chapman PB, Xu X, Sosman JA, McArthur GA, Ribas A, Kim KB, Grippo JF, and Flaherty KT (2009) PLX4032, a highly selective ^{V600E}BRAF kinase inhibitor: clinical correlation of activity with pharmacokinetic and pharmacodynamic parameters in a phase I trial. *J Clin Oncol (Meeting Abstracts)* **27 (Suppl):**9021.

Ring BJ, Chien JY, Adkison KK, Jones HM, Rowland M, Jones RD, Yates JW, Ku MS, Gibson CR, He H, et al. (2011) PhRMA CPCDC initiative on predictive models of human pharmacokinetics, part 3: comparative assessment of prediction methods of human clearance. *J Pharm Sci* **100:**4090–4110.

Roberts PJ and Der CJ (2007) Targeting the Raf-MEK-ERK mitogen-activated protein kinase cascade for the treatment of cancer. *Oncogene* **26:**3291–3310.

Rocchetti M, Del Bene F, Germani M, Fiorentini F, Poggesi I, Pesenti E, Magni P, and De Nicolao G (2009) Testing additivity of anticancer agents in pre-clinical studies: a PK/PD modelling approach. *Eur J Cancer* **45:**3336–3346.

Rosen L, LoRusso P, Ma WW, Goldman J, Weise A, Colevas AD, Adjei A, Yazji S, Shen A, Johnston S, et al. (2011) A first-in-human phase 1 study to evaluate the MEK1/2 inhibitor GDC-0973 administered daily in patients with advanced solid tumors (Abstract 4716). *Cancer Res* **71:**4716.

Salphati L, Pang J, Plise EG, Chou B, Halladay JS, Olivero AG, Rudewicz PJ, Tian Q, Wong S, and Zhang X (2011) Preclinical pharmacokinetics of the novel PI3K inhibitor GDC-0941 and prediction of its pharmacokinetics and efficacy in human. *Xenobiotica* **41:**1088–1099.

Simeoni M, Magni P, Cammia C, De Nicolao G, Croci V, Pesenti E, Germani M, Poggesi I, and Rocchetti M (2004) Predictive pharmacokinetic-pharmacodynamic modeling of tumor growth kinetics in xenograft models after administration of anticancer agents. *Cancer Res* **64:**1094–1101.

Solit DB, Garraway LA, Pratilas CA, Sawai A, Getz G, Basso A, Ye Q, Lobo JM, She Y, Osman I, et al. (2006) BRAF mutation predicts sensitivity to MEK inhibition. *Nature* **439:**358–362.

Tanaka C, O'Reilly T, Kovarik JM, Shand N, Hazell K, Judson I, Raymond E, Zumstein-Mecker S, Stephan C, Boulay A, et al. (2008) Identifying optimal biologic doses of everolimus (RAD001) in patients with cancer based on the modeling of preclinical and clinical pharmacokinetic and pharmacodynamic data. *J Clin Oncol* **26:**1596–1602.

Vuppugalla R, Marathe P, He H, Jones RD, Yates JW, Jones HM, Gibson CR, Chien JY, Ring BJ, Adkison KK, et al. (2011) PhRMA CPCDC initiative on predictive models of human pharmacokinetics, part 4: prediction of plasma concentration-time profiles in human from in vivo preclinical data by using the Wajima approach. *J Pharm Sci* **100:**4111–4126.

Wajima T, Yano Y, Fukumura K, and Oguma T (2004) Prediction of human pharmacokinetic profile in animal scale up based on normalizing time course profiles. *J Pharm Sci* **93:**1890–1900.

Wellbrock C, Karasarides M, and Marais R (2004) The RAF proteins take centre stage. *Nat Rev Mol Cell Biol* **5:**875–885.

Address correspondence to: Dr. Edna F. Choo, Department of Drug Metabolism and Pharmacokinetics, Genentech, Inc., 1 DNA Way, South San Francisco, CA 94080. E-mail: choo.edna@gene.com